Supporting Information

Switching Kinetics in Nanoscale Hafnium Oxide Based Ferroelectric Field-Effect Transistors

Halid Mulaosmanovic[1,], Johannes Ocker[1], Stefan Müller[1], Uwe Schroeder[1], Johannes Müller[2], Patrick Polakowski[2], Stefan Flachowsky[3], Ralf van Bentum[3], Thomas Mikolajick[1,4] and Stefan Slesazeck[1,*]*

[1] NaMLab gGmbH, 01187 Dresden, Germany

[2] Fraunhofer IPMS-CNT, 01099 Dresden, Germany

[3] GLOBALFOUNDRIES, 01109 Dresden, Germany

[4] Chair of Nanoelectronic Materials, TU Dresden, 01062 Dresden, Germany

Corresponding Authors

*E-mail: halid.mulaosmanovic@namlab.com

*E-mail: stefan.slesazeck@namlab.com

1. Polycrystalline nature of ferroelectric HfO_2

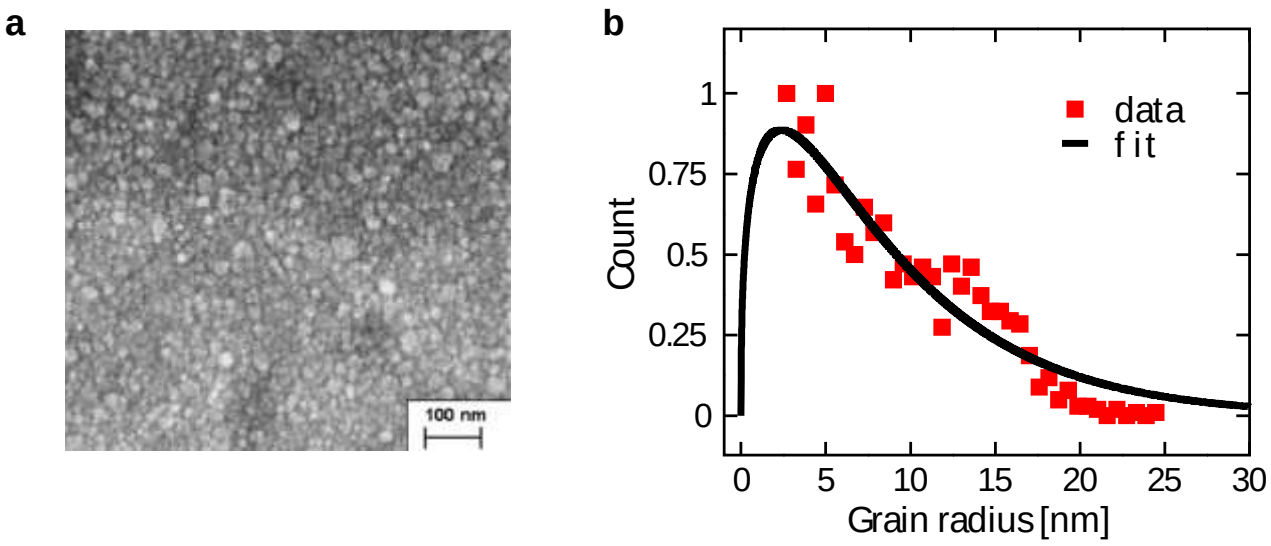

Figure S1: a, *Top-down SEM image of a ferroelectric polycrystalline Si:HfO_2 film having thickness 10 nm.* **b,** *Grain radius extracted from* **a,** *and the relative fit. Mean grain radius amounts to 10 nm approximately. Reproduced in part with permission from Ref. 41. Copyright 2016 IEEE.*

FeFET devices studied in this work are fabricated in a state-of-the-art 28nm high-k metal gate technology using a conventional gate first approach[1] (Figure 1a). A 1.2 nm nitrated thermal SiO_2 was grown on Silicon substrate followed by a 10 nm Silicon doped HfO_2 layer grown from $HfCl_4$ and $SiCl_4$ in a water based Atomic Layer Deposition (ALD) process at 300°C. TiN metallic gate was deposited with Physical Vapour Deposition (PVD) and contacted with poly-Silicon. The thermal budget for the complete gate stack reached a maximum temperature of 1050 °C at a spike activation anneal resulting in a fully crystalline Si:HfO_2 ferroelectric layer. The ferroelectric phase in HfO_2 is stabilized with a small Silicon concentration of approximately 4 mol%.

However, this fabrication method allowed for obtaining polycrystalline ferroelectric films. In fact, Figure 1b shows a top-view TEM micrograph of the HfO_2 film, once the gate electrode was removed, where several grains are clearly distinguishable. Analyzing the grain size distribution

from a similarly fabricated film shown in Figure S1a, a mean grain radius of around 10 nm was found[2]. Moreover, the portion of grains having the radius larger than 15 nm is not negligible. It is those grains that are able to stretch over the whole channel length and therefore exert, by means of their ferroelectric polarization charge, the greatest effect on the transistor channel conductivity.

The polycrystalline nature of the film has a substantial impact on the ferroelectric properties. First, domain walls cannot indefinitely propagate throughout the film as they would do in the bulk or epitaxial films. In a polycrystalline material they are constrained to remain within a grain.

It is well known that the ferroelectric domain structure is strongly dependent on grain size. Decreasing the grain size, the domain pattern becomes simpler and the number of domains within a grain decreases. Different groups reported for different ferroelectric polycrystalline materials a complete disappearance of multi-domain and the existence of only mono-domain grains when their size is smaller than 40 nm[3-5]. Therefore, we expect for our polycrystalline HfO_2 to have mono-domain grains.

Moreover, orientation, size and local variations of doping influence the amount of polarization charge and the direction of the polarization axis, creating in such a way rather a distribution of ferroelectric parameters (remanent polarization and coercive field) in large area devices.

2. Impossibility of *P*-*V* measurements

Measurements of the displacement current by applying a periodic AC voltage signal to the electrodes and its corresponding polarization-voltage (*P*-*V*) hysteresis are a conventional and relatively simple tool for the investigation of ferroelectric behavior. However, this kind of measurement is practically impossible for the assessment of switching of such a small number of domains in our ultra-scaled devices. In fact, the resulting displacement currents would appear too small to be captured by our measurement set-up. As a proof, we measured *P*-*V* hysteresis of large-

area transistors fabricated by the same process: these devices have area A=2*10^{-5} cm^2, which is 8.3*10^5 larger than our 80nmx30nm devices. As can be seen in the gate displacement current–gate voltage (I_G-V_G) plot in Figure S2a, the peak current is less than 200μA. If, instead, 80nmx30nm devices were measured, this current would be 200 μA/8.3*10^5=2.4*10^{-10}A, which turns out to be impossible to sense in this kind of transient measurement (10 kHz triangular waveform) and with the current set-up.

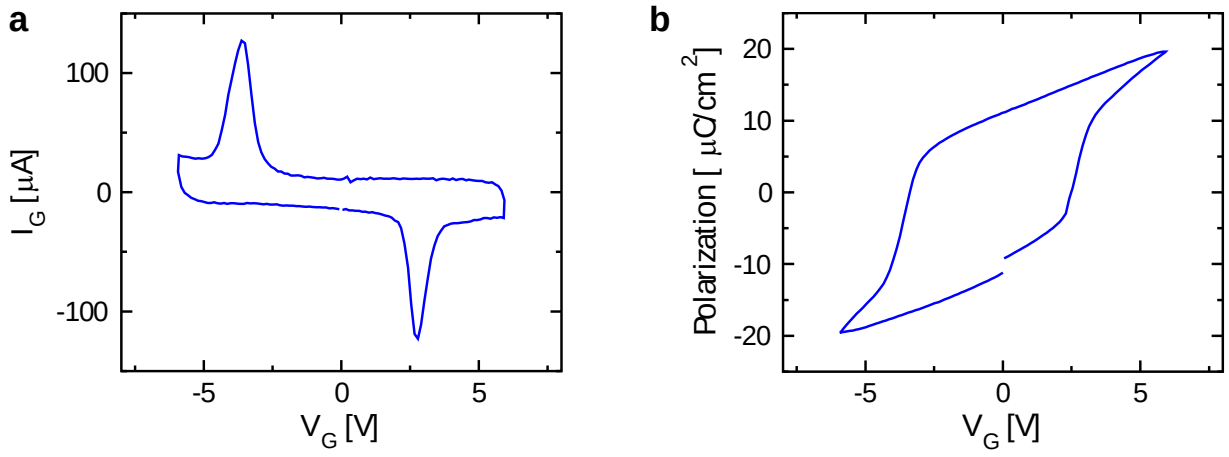

Figure S2: a, *Displacement current measured at the gate terminal of a large area FeFET upon applying a triangular voltage waveform.* **b,** *Corresponding P-V hysteresis obtained integrating the curve in* **a**.

3. Abrupt ferroelectric switching

Applying the gate voltage waveform of Figure 1e (inset), where V_P increases from 2 V to 5 V with a step of 50 mV, it is possible to observe very steep switching events in FeFET devices having the channel length of 30 nm (see Figure S3a-b). On the contrary, in large area devices, as for instance in Ref. 6 with L=10 μm and W=100 μm, the switching occurs only gradually upon the increase of the gate amplitude, stretching over a span of 3 V in Figures S3c and S3d. This strong contrast comes from the fact that the reduction of dimensions in the ultra-scaled devices has led to the presence of

only a few ferroelectric domains controlling the conductivity of the channel, whereas in 10 µm devices, a large number of domains displays rather a distribution of coercive fields resulting in a gradual transition from one polarization state to the other.

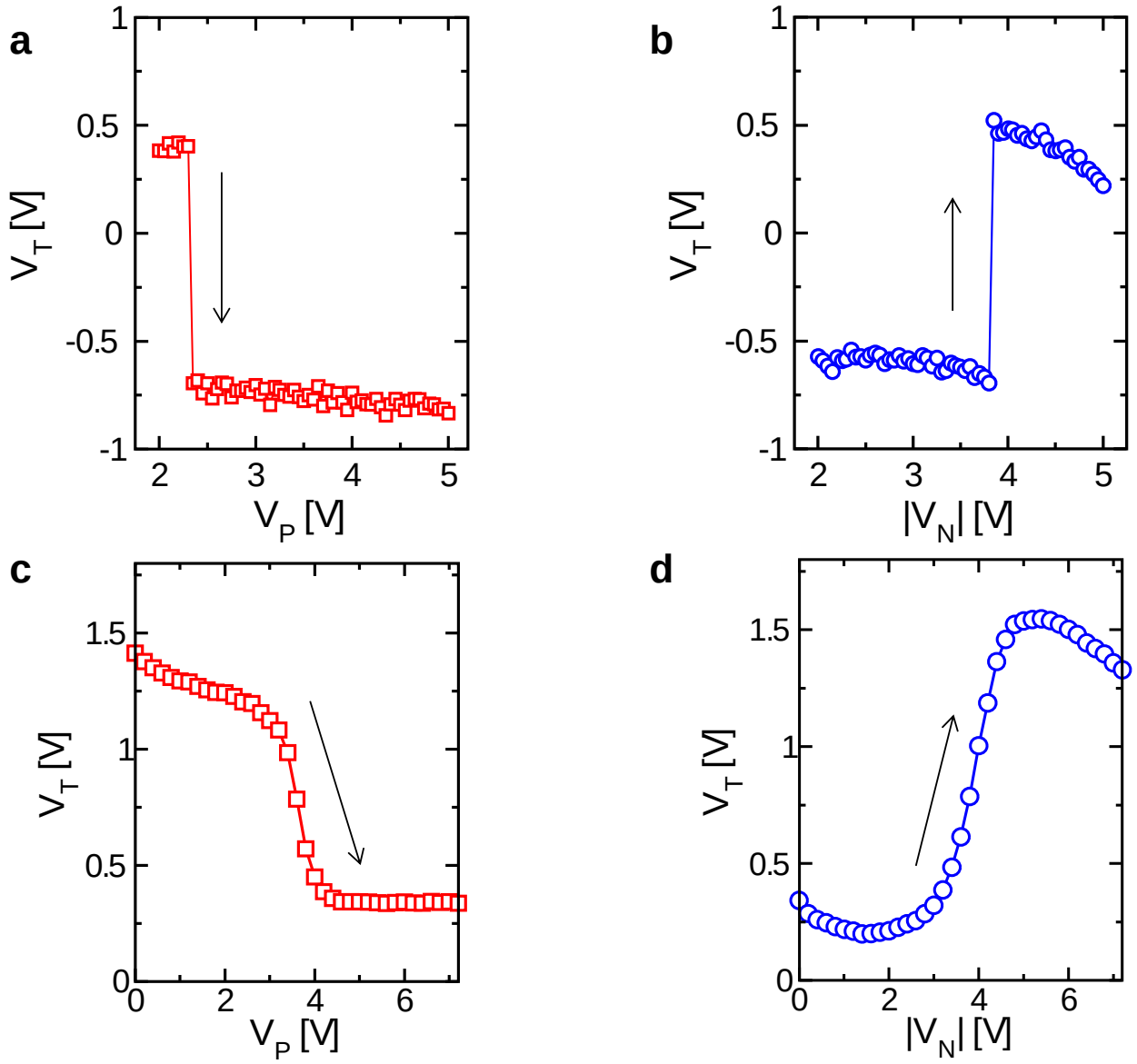

Figure S3: a, V_T *vs.* V_P and **b,** V_T *vs.* $|V_N|$ *graph of a FeFET having L=30 nm* **c,** *and* **d,** *same plots for a large area FeFET* [6] *having L=10 µm and W=100 µm.*

4. Nucleation mediated polarization switching

The formation of new ferroelectric domains can be treated by means of the classical nucleation theory (CNT) [7]. The CNT aims at quantifying the net rate at which the embryonic nuclei grow to a critical size, beyond which the new phase forms spontaneously[8]. Here, the nucleation process is described in terms of the change in Gibbs free energy of the system upon the formation of the new phase. Taking the free energy of the untransformed system as reference, the change in the Gibbs free energy when a nucleus forms, ΔG, is given by the sum of a bulk and a surface term:

$$\Delta G = \Delta g\, V + \gamma\, A \qquad \text{(S1)}$$

The first term at the right-hand side of Eq. (S1) represents the energy decrease upon the transition to a new phase, where V is the nucleus volume and Δg is the gain in free energy density ($\Delta g<0$), equal to $2 \cdot E \cdot P$, with E the applied electric field and P the switched polarization[9]. The second term represents the surface energy, where γ is the surface tension ($\gamma>0$) and in this case equal to the domain wall energy, and A is wall area of the nucleus.

Assuming a spherical nucleus with radius r, Eq. (S1) becomes:

$$\Delta G = \Delta g\, \tfrac{4}{3}\pi r^3 + \gamma\, 4\pi r^2 \qquad \text{(S2)}$$

For very small nuclei, the increase in the free energy due to formation of the new surface area ($\sim r^2$) dominates over the free energy decrease from bulk phase formation ($\sim r^3$), resulting in an energy barrier to nucleation. However, when the nucleus size exceeds the critical radius r^*, the bulk term dominates, leading to a decrease in ΔG. The free energy change ΔG reaches a maximum at r^*, denoted by ΔG^*, and the value of the critical nucleus can be determined by differentiation of Eq. (S2) with respect to r, obtaining

$$r^* = \frac{2\gamma}{\Delta g} \qquad \text{(S3)}$$

and the corresponding energy barrier height

$$\Delta G^* = \frac{16\pi\gamma^3}{3(\Delta g)^2} \qquad \text{(S4)}$$

The critical nucleus is in a metastable equilibrium with the surrounding untransformed phase at $\Delta G = \Delta G^*$. This means it has equal probabilities of growing or decaying and that the rate of nucleation in the system is therefore related to the rate of formation of these critical nuclei[10]. Only for $r > r^*$ the new nucleus can grow spontaneously. Within a framework of the theory of free energy fluctuations, the probability of a fluctuation in Gibbs free energy ΔG is proportional to $exp\left(-\Delta G/k_B T\right)$, where k_B is the Boltzmann's constant and T the temperature [10]. Therefore, the nucleation rate is given by

$$\lambda = \lambda_0 \cdot exp\left(\frac{-\Delta G^*}{k_B T}\right) \qquad \text{(S5)}$$

where λ_0 is the proportionality constant related to intrinsic properties of the material. The average waiting time for a nucleation event, which is the inverse of the nucleation rate λ, can be obtained by replacing ΔG^* in Eq. (S5) with the expression given in Eq. (S4) yielding

$$\tau = \frac{1}{\lambda} = \tau_0 \cdot exp\left(\frac{\alpha}{k_B T} \cdot \frac{1}{E^2}\right) \qquad \text{(S6)}$$

where $\tau_0 = 1/\lambda_0$ and represents the minimum nucleation time it is possible to reach and α is given by:

$$\alpha = \frac{4}{3}\pi\frac{\gamma^3}{P} \qquad \text{(S7)}$$

During the write operation in a FeFET device, the electric field E across the ferroelectric material, which appears in Eq. (S6), is proportional to the gate voltage, and therefore to the switching voltage

V_{SW} as well. The corresponding proportionality constant can be incorporated in α without loss of generality.

However, it is worthwhile to point out that additional effects might influence the nucleation process, including the depolarization field, charge trapping or elastostatic effects, which are not accounted for in Eq. (S1). Nevertheless, for the sake of simplicity, these will not be considered in this work. This simplification can be considered valid since the depolarization energy is expected to be negligible during the nucleation process[11]. Moreover, a special attention is paid to substantially reduce the charge trapping effects while studying the switching kinetics in Figure 4. This is done by considering the V_T *vs.* V_P instead of V_T *vs.* $|V_N|$ experiment. Indeed, as can be seen in Figure 3 in the main text, the experiment yielding V_T *vs.* V_P graphs, which correspond to the switching from high to low V_T state, exhibit a negligible charge trapping, in contrast to the V_T *vs.* $|V_N|$ experiment. In addition to this, the fast read operation described above helped in preventing the additional trapping.

5. Poisson process and fitting

Let us assume that the domain nucleation is a Poisson process[11] (Note that in the research area of crystal growth the nucleation is generally regarded as a Poisson process[12,13]). Then, its events (increments) are independent and stationary in time, occurring at rate λ, $\lambda>0$. Consequently, the time intervals elapsing between consecutive events, also called interarrival times, ΔT_i , $i=1,2,\ldots,$ are independent identically distributed exponential random variables having mean $1/\lambda$ as[14]:

$$p_{\Delta T_i} = \lambda\, e^{-\lambda\, \Delta T_i} \qquad \text{(S8)}$$

where $p_{\Delta T_i}$is the probability density function of ΔT_i . In our case, the rate λ is given by Eq. (S5). Moreover, independence between the events means that the formation of one nucleus does not influence the formation of the other nuclei within a grain and among other grains. Having this is

mind, the time required for the generation of *n* nuclei, also called the waiting time until the *n*th event occurs, is given by

$$t_{SW} = \sum_{i=1}^{n} \Delta T_i \ , \quad n \geq 1 \qquad \text{(S9)}$$

It is known that such a variable, t_{SW}, has a gamma distribution with parameters *n* and λ, having density given by[14]:

$$p_{t_{SW}}(t) = \ \lambda e^{-\lambda t} \frac{(\lambda t)^{n-1}}{(n-1)!} \ , \ t \geq 0 \qquad \text{(S10)}$$

which is characterized by the mean value and variance as given in Eqs. (S11) and (S12), respectively:

$$< t_{SW} >= \frac{n}{\lambda} \qquad \text{(S11)}$$

$$\sigma_{t_{SW}}{}^2 = \frac{n}{\lambda^2} \qquad \text{(S12)}$$

From the experimental data for $< t_{SW} >$ and $\sigma_{t_{SW}}$(reported in a graph shown in Figure 4c), it is straightforward to determine *n* and λ using Eqs. (S11) and (S12). In order to fit the experimental probability curves shown in Figure 4d, the Poisson process was simulated using MATLAB environment. By means of EXPRND function, *n* values of exponentially distributed ΔT_i interarrival times are randomly generated according to Eq. (S8), using *n* and λ as parameters (previously extracted as described above). Then, these ΔT_i values are summed up according to Eq. (S9). Repeating this procedure 20 times for each pulse width (t_{PW}) as in the experimental conditions, it is possible to obtain the simulated switching probability curves shown in Figure 4d by evaluating the probability:

$$P\left[t_{SW} \leq t_{PW}\right] \qquad \text{(S13)}$$

References:

(1) Müller, J.; Yurchuk, E.; Schlösser, T.; Paul, J.; Hoffmann, R.; Müller, S.; Martin, D; Slesazeck, S.; Polakowski, P.; Sundqvist, J.; Czernohorsky, M.; Seidel, K.; Kücher, P.; Boschke, R.; Trentzsch, M.; Gebauer, K.; Schröder, U.; Mikolajick, T. Ferroelectricity in HfO_2 Enables Nonvolatile Data Storage in 28 nm HKMG. *Symp. VLSI Technol., Dig. Tech. Pap.,* **2012**, 25-26.

(2) Mulaosmanovic, H.; Slesazeck, S.; Ocker, J.; Pesic, M.; Müller, S.; Flachowsky, S.; Müller, J.; Polakowski, P.; Paul, J.; Jansen, S.; Kolodinski, S.; Richter, C.; Piontek, S.; Schenk, T.; Kersch, A.; Künneth, C.; Bentum, R; Schröder, U.; Mikolajick, T. Evidence of Single Domain Switching in Hafnium Oxide based FeFETs: Enabler for Multi-Level FeFET Memory Cells. *IEEE Int. Electron Devices Meet.*, **2015**, 26.8.1-26.8.3.

(3) Roelofs, A.; Schneller, T.; Szot, K.; Waser, R. Piezoresponse Force Microscopy of Lead Titanate Nanograins Possibly Reaching the Limit of Ferroelectricity. *Appl. Phys. Lett.* **2002**, *81*, 5231-5233.

(4) Ren, S. B.; Lu, C. J.; Liu, J. S.; Shen, H. M.; Wang, Y. N. Size-related Ferroelectric-Domain-Structure Transition in a Polycrystalline $PbTiO_3$ Thin Film. *Phys. Rev. B*, **1996,** *54*, R14337.

(5) Frey, M. H.; Xu, Z.; Han, P.; Payne, D. A. The Role of Interfaces on an Apparent Grain Size Effect on the Dielectric Properties for Ferroelectric Barium Titanate Ceramics. *Ferroelectrics*, **1998**, *206(1)*, 337-353.

(6) Müller, J.; Böscke, T. S.; Schröder, U.; Hoffmann, R.; Mikolajick, T.; Frey, L. Nanosecond Polarization Switching and Long Retention in a Novel MFIS-FET Based on Ferroelectric HfO_2. *IEEE Electron Device Lett.* **2012,** *33 (2)*, 185-187.

(7) Du, X.; Chen, I. W. Frequency Spectra of Fatigue of PZT and other Ferroelectric Thin Films. *Mater. Res. Soc. Symp. Proc.* **1997**, *493*, 331.

(8) Debenedetti, P. G. *Metastable Liquids: Concepts and Principles* Ch. 3 (Princeton Univ. Press., Princeton, New Jersey, 1996).

(9) Merz, W. J. Domain Formation and Domain Wall Motions in Ferroelectric BaTiO3 Single Crystals. *Phys. Rev*. **1954**, *95*, 690–698.

(10) Ford, I. J. Statistical Mechanics of Nucleation: A Review. *J. Mech. Eng. Sci.*, **2004**, *218*, 883–899.

(11) Shin, Y.; Grinberg, I.; Chen, I.; Rappe, A. M. Nucleation and Growth Mechanism of Ferroelectric Domain-Wall Motion. *Nature* **2007**, *449,* 881-884.

(12) Goh, L.; Chen, K.; Bhamidi, V.; He, G.; Kee, N. C.; Kenis, P. J.; Zukoski III, C. F.; Braatz, R. D. A Stochastic Model for Nucleation Kinetics Determination in Droplet-Based Microfluidic Systems. *Cryst. Growth Des.*, **2010**, *10(6)*, 2515-2521.

(13) Jiang, S.; ter Horst, J. H. Crystal Nucleation Rates from Probability Distributions of Induction Times. *Cryst. Growth Des.*, **2010**, *11***,** 256-261.

(14) Ross, S. M. *Introduction to Probability Models*, Ch. 5 (10th ed. Academic Press, San Diego, California, 2009).